OTSU'S SEGMENTATION: REVIEW, VISUALIZATION AND ANALYSIS IN CONTEXT OF AXIAL BRAIN MR SLICES

**[1] HUMERA TARIQ, [2] ABDUL MUQEET, [3] AQIL BURNEY,
[4] MUHAMMAD AKHTER HAMID, [5] HUMERA AZAM**

[1]Assistant Professor, Department of Computer Science, University of Karachi, Pakistan
[2]Researcher, Image Processing and Machine Learning, Karachi, Pakistan
[3]Professor, Institute of Business Management, Department of Computer Science, Karachi, Pakistan
[4]Assistant Professor, Department of Paediatric, University of Toronto, Canada
[5]Lecturer, Department of Computer Science, University of Karachi, Pakistan

E-mail: [1] humera@uok.edu.pk , [2] abdulmuqeetcs@hotmail.com ,
[3] aqil.burney@iobm.edu.pk , [4]mahamid@rougevalley.ca, [5] humera.azam@uok.edu.pk

ABSTRACT

Otsu's Method is a non-parametric approach for image segmentation and is an attractive alternative to Bayes decision rule. Use of Nelder Mead for Otsu's optimization has been used since long but cannot be seen in image segmentation literature. We in this paper address this gap in a novel way and revive classical literature of Otsu's Image segmentation by experimenting it for voxel based tissue classification which then follows volume measurement of MRI base subjects. The other methods used to meet objective includes: spatial filtering, skull stripping and binarization of brain MR slices. The "goodness" of thresholds lies between $0.90 < \eta^* < 0.99$ for every brain MR slice in the volume. Significant difference was found (p<0.01) and (F >>1) amongst mean gray level of tissues, mean tissue volume densities within slices of each subject and in average volume tissue density of all Ten subjects.
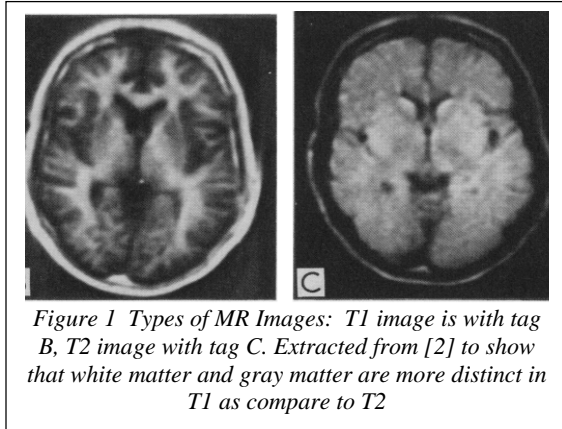
Keywords: *MR Brain Images, Otsu's Segmentation, Nelder-Mead Simplex Optimization, Image Segmentation, Volume Measurement, Skull Stripping, Tissue Classification*

1. INTRODUCTION

Background subtraction and discriminant analysis of foreground objects are two elementary requirements in object recognition, motion tracking and classification. In all such applications, the role of otsu' segmentation [1] is like an unavoidable rescue service that any one might needed to achieve mentioned tasks. This global segmentation approach is similar in functionality to clustering but it works in spatial space instead of feature space. We in this paper apply Otsu's segmentation to experiment with two main neuro imaging problems: skull stripping and tissue classification. Skull Stripping, also called Brain Extracion is a frequent preprocessing step in MRI image processing. This step removes meninges layer (tissues that pad the brain. (pia; arachnoid; dura) so that only main cerebrum is left in brain MR slice. Manual processs of skull stripping is quite labor intensive and requires skillful persons. Similar tissue classification is challenging due to ambiguity in gray levels of different tissue types. Tissue classification and volume measurement plays vital role in brain related disease diagnostics and determination of disease progression. We assume that the T1-weighted slice comprises of four tissues and thus each pixel of segmented regions can be assigned to any one tissue class. The classes are defined as background (BG), cerebrospinal fluid (CSF), gray matter (GM) and white matter (WM). It is very often to use term slice for an image representing either an axial, coronal or sagittal view of brain where a slice is just like a 2d image stored in matrix of size m x n. The smallest unit of slice is voxel meaning volumetric pixel. The difference in contrast in MR images arises from the fact that protons density at various tissues in human body differs. The two frequent types of brain MR images are T1 and T2 where the distinction is made on the basis of the time duration, from the instant when applied RF signal is removed till the instant when

nuclei precession of protons die out and they realign themselves with original magnetic field. A T1 image shows clear gray matter and white matter distinctions as compared to T2 image as shown in Figure 1 where the T2 image lacks in showing many anatomical details. The difference between contrasts is due to the chemical composition of myelin (like a dielectric material, a layer around neuron) in human brain.

Figure 1 Types of MR Images: T1 image is with tag B, T2 image with tag C. Extracted from [2] to show that white matter and gray matter are more distinct in T1 as compare to T2

Patient suffering from disease such as Multiple sclerosis have unmyelinated nerve tissues. Unmyelinated nerve tissues may also related to delayed neurological development in a child. Such pathologies (abnormalities) are much more visible in MR images. Readers are encourage to read previous effort in this work sequence [3][4].

We started with spatial filtering and peak valley analysis of multimodal histogram [5] for skull stripping which follows optimized Otsu's Thresholding [1][6] to determine three thresholds $k_1^*, k_2^*,\ k_3^*$ which separates the aforementioned regions. Visualization of Nelder Mead simplex is an interesting add on experience to study and learn. These optimal thresholds $k_1^*, k_2^*,$ k_3^* are used to obtain four binary images say $B_1, B_2, B_3\ and\ B_4$ respectively which provide us with CSF, GM and WM region voxels. To perform classification we employ connected component labeling and build discrete label matrix. Once label matrix is done, volume is measured by voxel counting processing over all slices of each ten subjects.

The rest of the paper is organized as follows: Section II provides an overview of underlying theory of Image segmentation followed by Otsu Thresholding, skull stripping, Nelder Mead Algorithm description and visualization in Section III. In Section IV, a recent application of Otsu's segmentation in context of Multispectral Adaptive

Region Growing Algorithm (MARGA) [31] has been discussed. The Experimental results and its discussion are presented in Section V. Finally the conclusion and future work is presented at the end in Section VI.

2. THEORY

A. Image Segmentation

In [6] the authors mentioned that the concept of region was first proposed by Marvin Minsky and Seymour Pappert. They described region as union of squares whose corners have minor or no difference in gray level. C.Brice and C.Finnema anticipate 'R' a region of the image if R is a connected set provided the topological structure is imposed by grid G of size M x N, thus R⊆G. They also showed that 4-neighbor connectivity principal of a pixel p, N4 (p) and gray level similarity based conditions led the basis of an equivalence relation on image pixels and it splits the image X=f(x,y) into a collection of disjoint subsets, where each subset contains pixels with specific intensity. For instance, in our case one subset contains all connected pixels that belong to Background (BG) and thus all are black, a second subset contains all dark gray pixels that belong to Cerebrospinal fluid (CSF), third subset is set of Gray Matter (GM) pixels and fourth subset is set of white matter (WM) pixels as shown in Figure 2. The collection of subsets forms a partition of X if it holds following relationships: x_i in a region R is connected to x_j if and only if there is a sequence $\{x_i, \ldots \ldots x_k \ldots \ldots x_j\}$ such that x_k and x_{k+1} are connected and all the points are in R. This means that three conditions must be fulfilled [7][8]:
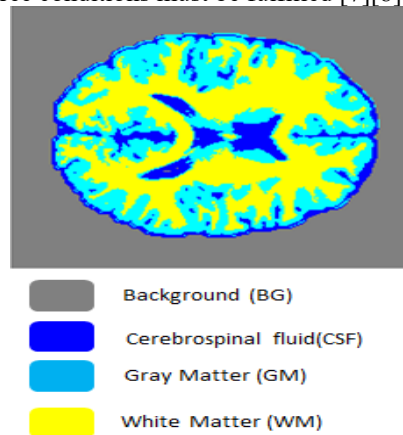

Background (BG)
Cerebrospinal fluid(CSF)
Gray Matter (GM)
White Matter (WM)

Figure 2 Regions as Connected Pixels

(i) $R_i \neq \emptyset\ for\ i \in I$
(ii) $R_i \cap R_j = \emptyset\ when\ i \neq j,$

(iii) $\bigcup_{i \in I} R_i = X$

Figure 3. Illustrates the concept of atomic regions of an arbitrary image. The arbitrary image f(x,y) is partitioned into four triangular subsets r_1,r_2,r_3,r_4   , the white boxes in Figure 3 illustrates the pattern of pixel connectivity within region. r_3 depicts 4-adjacency while r_1 r_2,and r_4   pixels follow 8- adjacency. Sophisticated addition of logical predicates to above region related facts led the foundation of most overwhelming problem of image processing domain, known as *image segmentation.*
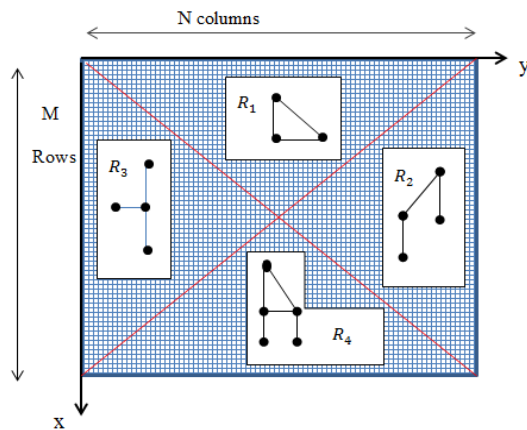
Figure 3 Pattern Of Pixel Connectivity Within Regions

Most segmentation algorithms follow either region formation or edge detection. Algorithms in the first category concentrates on abrupt change or discontinuity in image gray levels which corresponds to edges or boundaries between distinct regions while algorithms in second category focuses on similarity between regions for partitioning. Being a matter of fact, Region finding is dual of Edge finding as it is simple to derive a boundary from a connected set of pixels called regions and regions can be filled using edge information easily. The most standard image segmentation definition [8][9][10][11] irrespective of the type of input image is as follows: Let X is the set of all pixels and let P be the logical predicates defined on connected group of pixels to measure the region homogeneity then segmentation partitioned X into regions R_1, R_2, R_3,………R_(n)} such that:

(i) $\bigcup_{i \in I} R_i = X$ $i = 1,2,3 \dots \dots \dots . n$
(ii) $R_k \neq \emptyset$ $k = 1,2,3 \dots \dots \dots . n$
(iii) $R_i \cap R_j = \emptyset$ $when\ i \neq j,$
(iv) $P(R_k) = TRUE$ $k = 1,2 \dots \dots \dots \dots . n$
(v) $P\big(R_i \cup R_j\big) = FALSE$

$for\ i \neq j\ where\ R_i\ and\ R_j\ are\ adjacent$
Conditions (i), (ii) and (iii) follows from the definition of Equivalence relation on pixels as before where condition (i) indicates that every pixel in image must be assigned to some region or the whole is equal to the sum of its parts, this is called Completeness. Completeness property means that the segmentation algorithm terminates only when every pixel is processed. Condition (ii) makes sure that at least one region must exist. Condition (iii) indicates that it is not possible that two different regions (disjoint regions) share the same pixel. This is called distinctness. Condition (iv) depicts that a certain predefined similarity or homogeneity criteria must be fulfilled for all regions. Finally, the Condition (v) makes sure that a homogeneity criterion is never true when applied to union of two adjacent regions. This is to show that a region is composed of maximal connected pixels. Various Surveys have been conducted on Image Segmentation [9][12][10][14] and also on Brain MR Image Segmentation as well [18][13][14]. Image Segmentation surveys covers the broader aspects of segmentation techniques irrespective of its type of image (or discusses different types of images) while Brain MR is simply an in-depth and more focused survey as type of input image is already known. Zucker [9] examined five approaches to region growing techniques which include: (1) Regional neighbor search, (2) Multi-regional heuristic, (3) Functional approximation and merging, (4) Split and merge, (5) Semantics. He came into limelight the two important issues of Threshold selection and Order dependency in case of Region Growing algorithms. Haralick and Linda G. Shapiro [12] categorized segmentation techniques into six classes: (1) Measurement space guided spatial clustering (2) Thresholding (3) Multidimensional Measurement Space clustering (4) Region Growing (5) Spatial Clustering and (6) Split and Merge. They view segmentation as clustering problem in measurement space, where measurement space methods are simply histogram based techniques for partitioning. N.R Pal and Sankar K. Pal [10] extend the segmentation survey further to discussion of Iterative Pixel Classification which include (1) Relaxation (2) MRF based approaches (3) Neural Network based approaches, Surface based segmentation and fuzzy segmentation techniques [10]. An exhaustive survey on thresholding techniques is been conducted in which 40 thresholded methods are compared using non-destructive testing [15], amongst them otsu's algorithm ranks 6.

Segmentation of medical images (CT, MRI) is much more challenging due to typical image acquisition artifacts. The major artifact that are been investigated by many researchers are intensity inhomogeneity (bias field) [16][17]. This multiplicative bias field is modeled and estimated by various techniques including Bayesian approach (EM algorithm) [18], Entropy Minimization methods [19], Level set methods [20] and Fuzzy C-Means [21]. Another major MR imaging artifact is partial volume effect which is misclassification of voxels especially at boundaries [22]. Readers are encouraged to see references [23][24][14] for reviewing methods and details of Brain MR Image segmentation.

B. Otsu's Multithresholding

The objective in otsu's method [1] is maximization of between class variance to obtain optimum threshold(s) giving the best separation amongst desired groups or classes. The method is an attractive alternative to parametric methods which requires some definite workable assumptions about PDF estimation for e.g. gray levels follows Gaussian distribution which is not the case in brain MR slices. The non-parametric methods are also robust against noise which is inherent problem of brain MR data. Suppose we segment the input gray levels into K classes $C_1, C_2, C_3, \dots \dots \dots C_K$ where C_1 consist of all the gray levels in the range$[0, k_1]$, C_2 consist of all the gray levels in the range $[k_1, k_2]$ and similarly the class C_K consist of all the gray levels in range$[k_{k-1}, L-1]$. The K classes requires $K-1$ thresholds with values, $k_1^*, k_2^*, \dots \dots k_{K-1}^*$ such that the between class variance becomes maximized. The generalize expression for between class variance σ_B^2, with two or more classes is:

$$\sigma_B^2 = \sum_{k=1}^{K} \omega_k (\mu_k - \mu_G)^2 \qquad (1)$$

Where ω_k, μ_k and μ_G represents probability of occurrence of class C_K (or the cumulative sum), the mean value of gray levels thresholded into class C_K and the global mean respectively. The respective expressions for these statistics are given as follows:

$$\omega_k = \sum_{i \in C_K} p_i \qquad (2)$$

$$\mu_k = \frac{1}{\omega_k} \sum_{i \in C_K} i \cdot p_i \qquad (3)$$

$$\mu_G = \sum_{i=0}^{L-1} i \cdot p_i \qquad (4)$$

The following relationship must hold when ω and μ terms are substituted in following:

$$\sum_{C_K} \omega_k \mu_k = \mu_G \qquad (5)$$

$$\sum_{C_K} \omega_k = 1 \qquad (6)$$

It is obvious that ω and μ terms are functions of $k_1, k_2, \dots \dots k_{K-1}$ and thus σ_B^2 also is. The K-1 optimum thresholds are the values that maximizes between class variance $\sigma_B^2(k_1, k_2, \dots \dots k_{K-1})$ and are determined by finding:

$$\sigma_B^2(k_1^*, k_2^*, \dots k_{K-1}^*) = \max_{0 < k_1 < k_2 \dots < k_{K-1} < L-1} \sigma_B^2(k_1, k_2, \dots k_{K-1})$$
$$(7)$$

The goodness of $K-1$ optimal thresholds is determine by measuring class separability used in discriminant analysis [25] and is obtained by evaluating following equation at optimal thresholds:

$$\eta = \frac{\sigma_B^2}{\sigma_w^2} \qquad (8)$$

Where

$$\sigma_B^2 = \sum_{k=1}^{K} \omega_k (\mu_k - \mu_G)^2 \qquad (9)$$

$$\sigma_w^2 = \sum_{k=1}^{K} \omega_k \sigma_k^2 \qquad (10)$$

σ_B^2 is the already discussed as between class variance while σ_w^2 represents within class variance and is given by following expression:

$$\sigma_k^2 = \sum_{i \in C_K} (i - \mu_k)^2 \qquad (9)$$

C. Nelder-Mead Downhill Simplex Method

Our main objective in segmentation is basically, to solve the following maximization problem:

$$\max_{0 < k_1 < k_2 \dots \dots < k_{K-1} < L-1} \sigma_B^2(k_1, k_2, \dots \dots k_{K-1})$$

Subject to the constraints $k_1, k_2, \dots \dots k_{K-1} \geq 0$
Where σ_B^2 is between class variance. The Nelder Mead Simplex algorithm [6][26] is a direct search method for optimization of a function of more than one variable. It starts with an initial simplex which is a polygon or a polyhedron depending on the dimension you are dealing with. For example in case of brain MR images the initial simplex is a

tetrahedron in $\mathbb{R}^3$ as we need to determine three thresholds (n=3) to segment the brain slice into four classes. Generally speaking, in n-dimension the algorithm starts with a non- degenerate simplex having n+1 vertices. Here non-degenerate means that the simplex must enclose a non-zero volume. Function to be minimized is evaluated at all n+1 points and are arranged accordingly so that $f(x_1) \leq f(x_2) \leq \cdots .... \leq f(x_{n+1})$. The idea is to replace $f(x_{n+1})$ with a new point so that it gives a smaller value. This new point is determined, updated and moved in space by a series and combination of steps namely, reflection, expansion and contraction so that the new simplex have better set of points. The formal Nelder mead algorithm comprises of following steps:

Initialization Function values are evaluated at initial simplex vertices:

$$f_i^{(1)} = f(x_i)^{(1)} \qquad i = 1,2 ..... n+1$$

Repeat:
(1) Sorting: Order the simplex vertices such that
$$f_1^k \leq f_2^k \leq \cdots ...... \leq f_{n+1}^k$$

(2) Reflection: Reflect the worst point with respect to centroid of n points as follows:

$$\overline{x}^{(k)} = \frac{1}{n} \sum_{i=1}^{n} x_i^{(k)}$$

$$x_r^{(k)} = \overline{x}^{(k)} + (\overline{x}^{(k)} - x_{n+1}^{(k)})$$

Evaluate function at reflection point i.e.

$f_r^{(k)} = f(x_r^{(k)})$ and compare it with current best such that: IF $f_1^{(k)} \leq f_r^{(k)} \leq f_n^{(k)}$

ACCEPT $x_r^{(k)}$ and check convergence at step (6).
END
END

 (3) Expansion: Check the following criteria
IF $f_r^{(k)} < f_1^{(k)}$
Calculate Expansion
$$x_e^{(k)} = \overline{x}^{(k)} + 2(x_r^{(k)} - \overline{x}^{(k)})$$

Evaluate $f_e^{(k)} = f(x_e^{(k)})$

IF $f_e^{(k)} < f_r^{(k)}$
 ACCEPT $x_e^{(k)}$ and check convergence at step (6).
END
END

(4) Contraction: Check the following criteria
IF $f_r^{(k)} \geq f_n^{(k)}$
IF $f_r^{(k)} < f_{n+1}^{(k)}$
Calculate Contraction
$$x_c^{(k)} = \overline{x}^{(k)} + \frac{1}{2}(x_r^{(k)} - \overline{x}^{(k)})$$

Evaluate $f_c^{(k)} = f(x_c^{(k)})$
IF $f_c^{(k)} < f_r^{(k)}$
ACCEPT $x_c^{(k)}$ and check convergence at step (6).
END
ELSE IF $f_r^{(k)} \geq f_{n+1}^{(k)}$

Calculate Contraction
$$x_c^{(k)} = \overline{x}^{(k)} - \frac{1}{2}(x_r^{(k)} - x_{n+1}^{(k)})$$
Evaluate $f_c^{(k)} = f(x_c^{(k)})$
IF $f_c^{(k)} < f_{n+1}^{(k)}$
ACCEPT $x_c^{(k)}$ and check convergence at step (6).
END
END
END
Note there are two types of contractions: First one is named *outside contraction* which contracts x_(n+1) halfway towards the centroid to yield better point while the second is named inside contraction which contracts all points halfway towards first point.
(5) Shrink: This step moves all vertices of simplex except the best (or minimum) as follows

$$v_i^{(k)} = x_1^{(k)} + \frac{1}{2}\left(x_i^{(k)} - x_1^{(k)}\right),$$

Where $i = 1,2 , ... n+1$

Evaluate: $f_i^{(k)} = f(v_i^{(k)})$, i= 1,2…n+1

ACCEPT $v_i^{(k)}$ as updated vertices.
(6) Convergence
Two conditions should be checked for convergence criteria:
a) If the maximum coordinate difference between the current best point and the other points in the simplex is less than or equal to some predefined tolerance say $1e^{-4}$. This condition says that repeat until:

max (‖x2-x1‖,‖x2-x1‖,...,‖x(n+1)-x1‖) <= $1e^{-4}$

Where ‖.‖ is the infinity-norm, and v1 holds the vertex with the current minimum value;

b) According to second condition the corresponding difference in function values is less than or equal to $1e^{-4}$. The iteration stops when the maximum number of iterations reached or function evaluations are exceeded.

3.   EXPERIMENTATION

A. MR Data Acquisition

Analysis has been done on brain MR simulated volume generated with the Internet connected MRI Simulator at the McConnell Brain Imaging Centre in Montreal [27]. We choose to download ten datasets with different noise and intensity non-uniformity (INU) levels. The files are in raw short (12 bit) format and are named according to their noise level and INU for e.g. the possible noise levels and INU are {1,3,5,7,9} and {20,40} percent respectively. All volume spans 181x217x181 in x, y and z axis respectively. This means each volume is comprising 181 x 217 brain slices as we move for example in z-direction. The slice thickness is 1mm showing each voxel volume is $1\ mm^3$. The three ways to analyze brain volume is to move forward in three different directions along x, y and z. As an example, the brain slice corresponds to a particular x, y, z in 3D space is shown in   Figure 4 Row 1, in which sagittal view corresponds to slice in yz plane, coronal view corresponds to slice in xy plane while axial view corresponds to slice lying in xz plane. The intuitive representation of these planes along with corresponding slices is shown in Figure 4 Row 2. Readers should note that one has to analyze and process all volume slices in any one direction usually taken as z or axial slices. Also note that extreme slices are very much different from middle slices which affect and harm processing results.
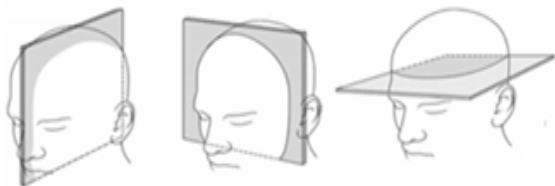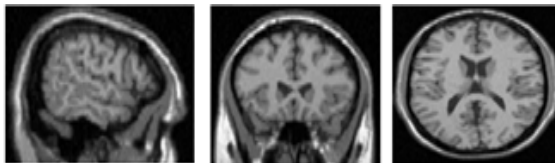
Figure 4 (a) Row1: sagittal slice, coronal slice, axial Slice Figure 4(b) Row2: sagittal plane, coronal plane, axial-plane.
http://link.springer.com/chapter/10.1007/978-1-60761-250-6_1

B. Spatial Filtering

We discussed in previous section that the MR data under consideration comprises of ten subjects with 181 slices of 217 x181 voxels each. All the ten subjects differ from each other with respect to noise and intensity non-uniformity INU such that we have total 10 combination made from {1,3,5,7,9} and {20,40} respectively. The intensity inhomogeneity is an inherent artifact in MRI image formation due to variation in magnetic field while noise in MR data gives an impression of impulse kind of noise, see Figure 5(a). To deal with such random noise and inhomogeneity medial filter is an appropriate choice as it replaces the gray level of current voxel by the median of surrounding neighborhood with considerably less blurring. The replacement of central or current pixel with median formulation is given below while the results of filtering are shown in Figure 5(b).

$$g(x,y) = \underset{N}{\text{median}}\{f(x,y)\} \qquad (11)$$

Where $f(x,y)$ is noisy MR image, $g(x,y)$ is filtered image while N represents neighborhood of specific size around central pixel. Literature shows that noise in MR images follows Rician distribution for which non-local mean parametric filter does successful denoising but it takes much more time than median filtering [28][29].

C. Skull Stripping

A background threshold is applied to create an initial brain mask. This initial mask is processed by certain morphological operation to create another binary mask that has ones only at regions representing cerebrum. Element wise multiplication of second mask with original brain image yields the central brain without hard skull. The thresholding process for skull stripping requires histogram analysis of original axial slice. The pixels corresponding to unique gray levels have been counted to build histogram of axial slices which is then smoothed using 1-d Gaussian Window. The original multimodal histogram is shown in Figure 6; whereas its smoothed version along with peaks and valley is shown in Figure 7.
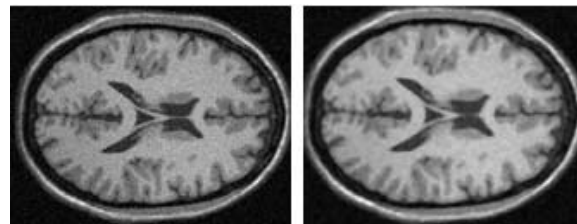

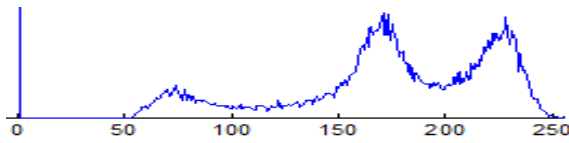**Figure 5 (a) Noisy MR Image   (b) Median Filtered Image**

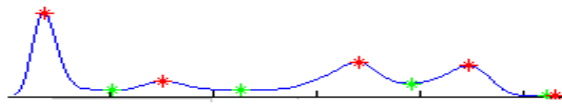*Figure 6 Multimodal Histogram Of Brain Axial Slice*

Figure 7 Peak And Valleys Of Multimodal Histogram

To separate skull from brain the very first valley has been extracted via smoothed histogram peak and valley analysis [5]. Morphological operations include opening with a disk structuring element of appropriate radius which shrinks the image by stripping away layer of pixels from outer boundaries of brain region and as a result of multiplying it with original we get skull stripped image of axial slice. The process is repeated for the whole volume of brain and for all datasets. Note that the size of disk structuring element needs to vary such that it is workable for maximum number of slices in the brain to be processed. The steps for skull stripping are shown in Figure 8. Figure 8 (a) is the original axial slice, Figure 8(b) is the binary mask (named as Mask I) obtained by applying first valley threshold in histogram, Figure 8(c) is our second mask (named as Mask II) obtained by opening the first mask. Figure 8(d) shows brain without skull.
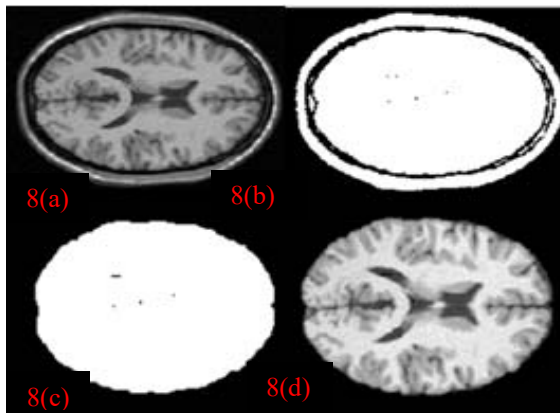
Figure 8 (A) Slice (B) Mask I (C) Mask II (D) Cerebrum

D. Optimization and Thresholding

The objective here is to segment the axial brain slice into four regions($k = 4$), the dark background BG, the dark gray cerebrospinal fluid CSF, the gray matter GM and the brightest white matter region using thresholding technique. The histogram of axial slice clearly shows four peaks (see Figure 7). It's a multimodal histogram, thus

three thresholds k_1, k_2 and k_3 should exist to partition the entire histogram into four. The highest peak in histogram represents the background comprising of pixels/voxels having lowest gray levels. Whatever is left after excluding these background pixels is our brain. This suggests that all pixels above certain threshold can be considered to belong to the head. Since some noise is always present, so a percentage of adjacent CSF pixels are also identified as part of background BG and same misclassification occurs at boundary between CSF and GM, and between GM and WM. The problem is named in literature as partial volume effect [22]. Apart from the background peak three more peaks exist which corresponds to different image intensities of the tissue classes. As input slices differ in intensity and noise therefore the three thresholds can be varied. In poorer contrast image, the peaks would flux with each other would cause segmentation, a more challenging task. All the pixels of the CSF in the slice have their values in the area of the second peak of skull stripped brain, the pixels of the GM matter lay under the area of third peak and similarly the brightest gray levels correspond to WM which lay in the fourth and final peak of histogram. Since a number of pixels which are part of the skin and other tissues may have values within the range of these peaks, thresholding might yield an inappropriate segmentation especially when if one only relies on peak and valleys of histogram.

Two procedures have been adopted to determine optimal thresholds $T1^*, T2^*$ and $T3^*$. First we attempt peak and valley analysis ([5]) of multi modal histogram of Figure 6, as we previously did in skull stripping. The smooth version of peak and valleys can be seen in Figure 7 where red markers indicate peaks for Background (BG), Cerebrospinal fluid (CSF), Gray matter (GM) and White matter (WM) respectively whereas the green markers are the respective valleys. We use valleys to extract the four regions and it seems that valley thresholds separate histogram modes very well. The result in Figure 9(b) is obtained by smoothing the brain slice using Gaussian filter which is a workable assumption [30]. To specify the size of Gaussian filter, recall that in a multi-modal histogram about 75% of the pixels lie between $\pm 3\sigma$ about the mean. The thresholds obtained this way lie in the three valley area of smooth histogram and provide us with following segmented image:
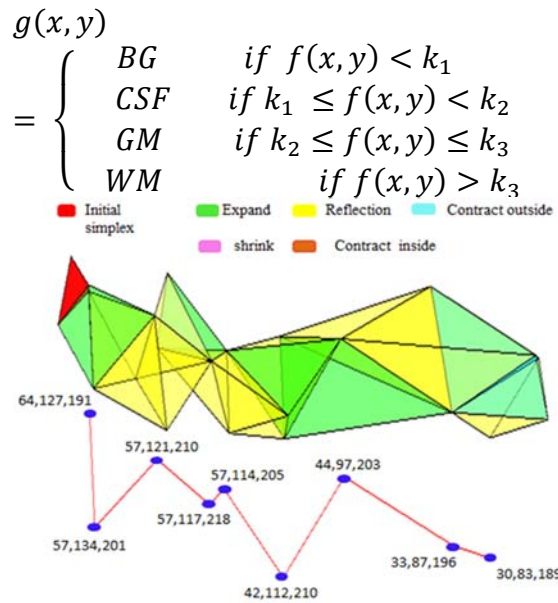
$$g(x, y)$$
$$= \begin{cases} BG & if \ f(x,y) < k_1 \\ CSF & if \ k_1 \leq f(x,y) < k_2 \\ GM & if \ k_2 \leq f(x,y) \leq k_3 \\ WM & if \ f(x,y) > k_3 \end{cases}$$

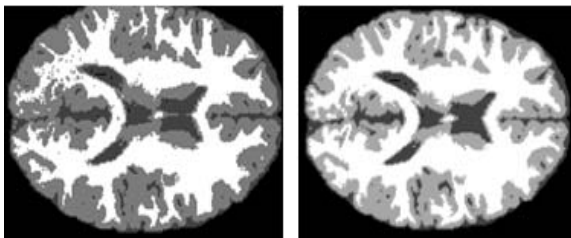*Figure 9 Nelder Mead Optimization In* $\mathbb{R}^3$

Figure 10 (A) Peak Valley Segmentation (B) Otsu's Segmentation

One can easily realize that it is difficult to detect the valleys precisely, because valleys are flat and broad and the peaks are unequal in height, making valleys untraceable. One of the peak and valley based segmented image is displayed in Figure 9(a) but for entire brain volume this derivative based peak valley method fails as all slices within a volume needs different value for peak detection. So *Unconstrained Nonlinear Optimization method* is used which is commonly known as Nelder Mead method or downhill simplex method [6]. Figure 9(b) shows the segmented image where thresholds are obtained from Nelder Mead method; the result is thus an improved version in comparison to Figure 9(a). Possible optimization steps of the downhill simplex algorithm in $\mathbb{R}^3$ in search of best possible thresholds that separates the four classes in brain MR images with three thresholds namely k_1, k_2 and k_3 are illustrated in Figure 10. The steps allow the tetrahedron to move in space at every iteration via reflection, expansion, inside contraction, outside contraction and shrink operations. We have used different colors to show

each operation on simplex in 3D space, see Figure 10. The geometrical simplex (tetrahedron) can adapt to the surface of function $f = \sigma_B^2$ where σ_B^2 means between class variance, a very well-known measure for statistical discriminant analysis. When minimum point is far from minimum, the expansion step allows the tetrahedron to move in the descent direction. On the other hand, when the minimum is inside the tetrahedron, contraction and shrink steps allow vertices to be moved closer to it. Figure 10 also demonstrates the search path for complete iteration of down-hill simplex method along on xz plane. The 2D projection is a much better tool to have a look at search direction and step length. In Figure 10 the initial simple is shown in red with initial guess threshold of (64,127,191). A series of such expansions and reflections in three dimensional space along search path goes through:

(57,134,201),(57,121,210),(57,117,218),(57,114,205),(42,112,210),(44,97,203),(33,87,196)   and (30,83,189).

There is no shrink and inside contraction occur in this particular iteration. Most of the time the search utilizes the expansion and reflection operations to reach to the minima I this case. More iterations of downhill simplex are tabulated in Table I ahead in the paper for better visualization and understanding of Simplex method.

E. Binarization

To create masks from an image having more than one gray level, one has to mainly go through connected component (CC) analysis of segmented regions. The Otsu's thresholds k_1^* k_2^*, and k_3^* obtained in previous step are applied on multi-threshold segmented image one by one to obtain four binary images shown in Figure. 11. Figure 11(a) shows whole brain surface as white area and rest of the pixel represents background i.e. $f(x, y) < k_1^*$. Binary Image in Figure 11(b) represents region where $k_1^* < f(x, y) < k_2^*$ and it clearly contains pixels that consist of CSF and GM together in one image while Binary Image in Figure 11(c) is the segmented WM region for which $k_2^* < f(x, y) < k_3^*$. Processing of these binary images obtained after applying multiple thresholds needs combining some morphological processing as well to achieve reliable segmentation. For example, it is important to get rid of the parasitic components "spurs". In our context spurs are caused during labeling of binary images by non-uniformities of gray levels in the segmented image.

It is also important to pick up the "tips" of parasitic branches and eliminate them. It has to be noted that some of these eliminated spurs and branches are picked up again during dilation because they are valid pixels of regions. The results of these binary operations are shown in Figure 11(d) till Figure 11(f). To separate CSF and GM as they are in one image (see Figure 11(b), we use histogram thresholding. These binary images would help a lot in label matrix creation and volume measurements but it is difficult to create all these masks in a fully automatic fashion. Another simple strategy is to determine unique gray levels in the segmented image and assigning them the desired class labels. This uniformly runs over entire brain volume and we get the corresponding label matrix for each slice. This label matrix creation completes our segmentation and classification step whose sample results are shown in Figure 12. The dark gray areas in Figure 12 corresponds to BG means label 0, the blue areas correspond to CSF whose label is 1, the GM region is shown in cyan and has label 3; finally, WM is shown in yellow and is assigned label 4.

F. Volume Measurements

The objective here is to determine brain and non-brain voxels and to calculate volume occupied by CSF voxels, GM voxels and WM voxels in the ten phantom data sets.
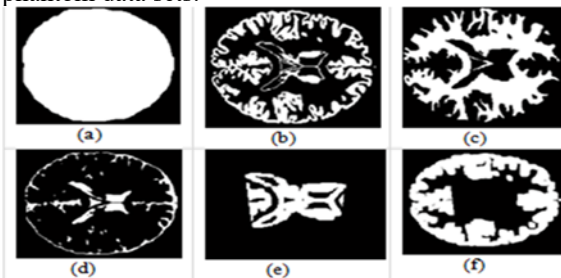
Figure 11 Binary Images Obtained By Otsu's Segmentation
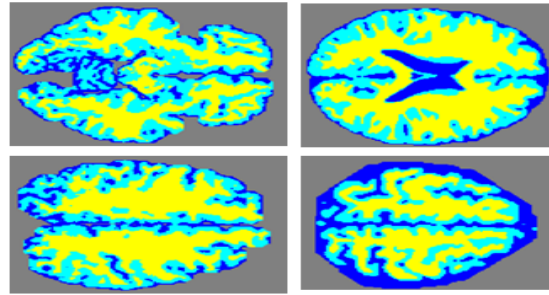
Figure 12 Labeling And Voxel Classification

The brain voxels in an MRI dataset are determined by taking summation of brain volumes over all slices, where brain volume of each slice is the product of brain voxel count in that slice and voxel size. The volume of a single brain MR data V_B is expressed as:

$$V_B = \sum_{slices}(n * V_{voxel}) \qquad (12)$$

$$V_{CSF} = \sum_{slices}(n_1 * V_{voxel}) \qquad (13)$$

Where n voxel is count per slice and V_{voxel} represents the volume of an individual voxel in slice. The voxel counting process is done with the help of label matrix created at binarization stage. Volume density of a particular tissue in all slices of a single brain volume is measured to determine total tissue density with in a subject and can be expressed as:

$$V_{GM} = \sum_{slices}(n_2 * V_{voxel}) \qquad (14)$$

$$V_{WM} = \sum_{slices}(n_3 * V_{voxel}) \qquad (15)$$

Where n_1, n_2, n_3 are voxel count for CSF, GM and WM respectively and since we assume that all pixel either belong to background BG ore any one of this tissue, therefore:

$$n = n_1 + n_2 + n_3 \qquad (16)$$

Table 1 Skull Stripping Challenge Of Different Brain Subjects

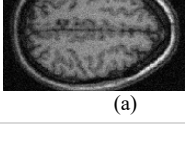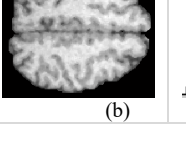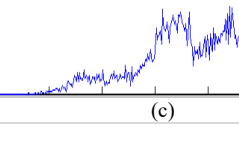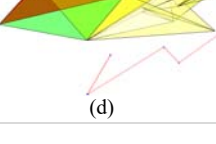| Subject No. Slice No.	Original Slice	Skull Stripped Brain	Multimodal Histogram	Optimization	Otsu's thresholds and σ_B^2
Subject I Slice 50	(a)	(b)	(c)	(d)	$k_1^* = 51$ $k_2^* = 117$ $k_3^* = 181$ $\eta = 0.9265$ (e)
Subject I Slice 90	(a)	(b)	(c)	(d)	$k_1^* = 53$ $k_2^* = 132$ $k_3^* = 205$ $\eta = 0.9906$ (e)
Subject I Slice 140	(a)	(b)	(c)	(d)	$k_1^* = 53$ $k_2^* = 127$ $k_3^* = 200$ $\eta = 0.9883$ (e)
Subject V Slice 50	(a)	(b)	(c)	(d)	$k_1^* = 27$ $k_2^* = 74$ $k_3^* = 125$ $\eta = 0.970$ (e)
Subject V Slice 90	(a)	(b)	(c)	(d)	$k_1^* = 51$ $k_2^* = 122$ $k_3^* = 185$ $\eta = 0.99$ (e)
Subject V Slice 140	(a)	(b)	(c)	(d)	$k_1^* = 46$ $k_2^* = 124$ $k_3^* = 188$ $\eta = 0.99$ (e)
Subject X Slice 50	(a)	(b)	(c)	(d)	$k_1^* = 56$ $k_2^* = 152$ $k_3^* = 187$ $\eta = 0.99$ (e)
Subject X Slice 90	(a)	(b)	(c)	(d)	$k_1^* = 49$ $k_2^* = 161$ $k_3^* = 193$ $\eta = 0.99$ (e)
Subject X Slice 120	(a)	(b)	(c)	(d)	$k_1^* = 61$ $k_2^* = 139$ $k_3^* = 178$ $\eta = 0.99$ (e)
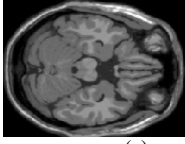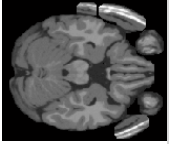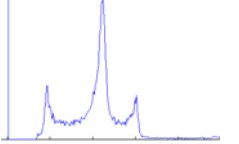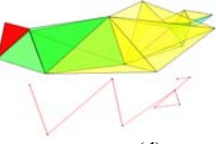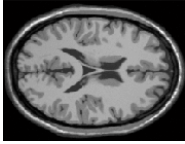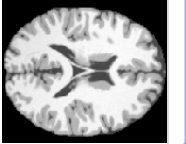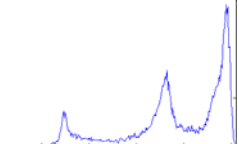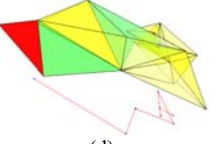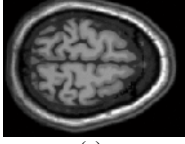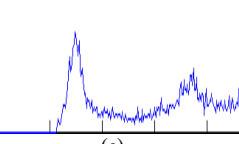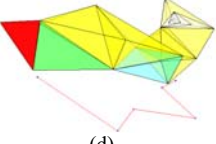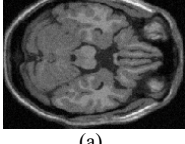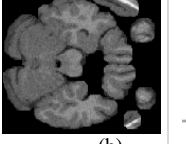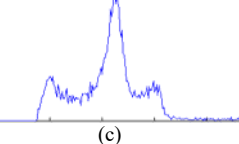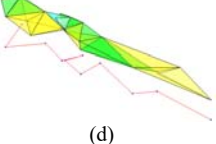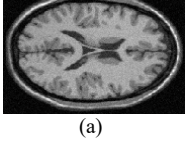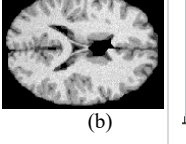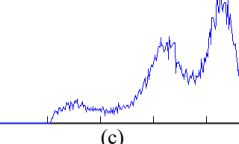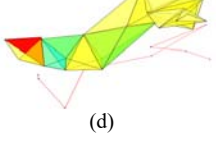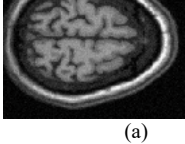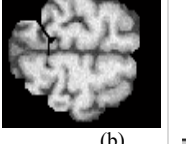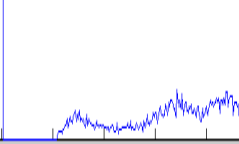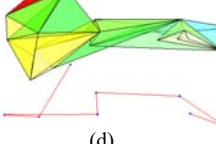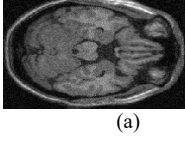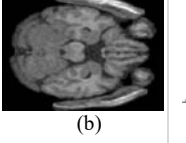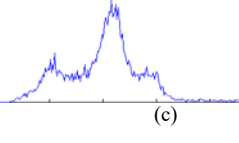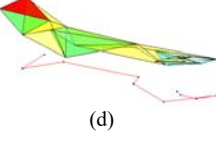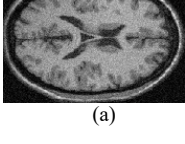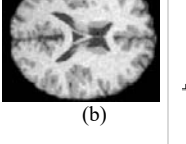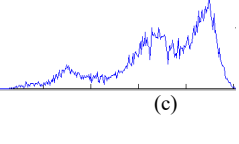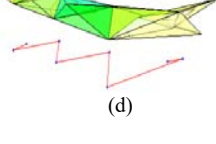
MR tissue density can be estimated as the ratio of tissue volume to total volume of the brain and thus is given by:

$$D_{tissue} = \frac{V_{tissue}}{V_B} \qquad (18)$$

Where tissue may replace {CSF, GM, WM} and thus D_{tissue} refers the respective tissue density. After each brain volume measurements results can be combined to measure total tissue volume densities over all subjects under consideration for analysis as follows:

$$D_{total\ CSF} = \sum_{brain\ volume} V_{CSF} \qquad (19)$$

$$D_{total\ WM} = \sum_{brain\ volume} V_{wM} \qquad (20)$$

$$D_{total\ WM} = \sum_{brain\ volume} V_{wM} \qquad (21)$$

4. OTSU'S METHOD IN MEDICAL IMAGING

The two recent and important work on structural brain MR Images are [31][32]. Both addresses Skull Stripping problem where [32] claims to be more robust than [31] in the presence of some pathology in brain. The purpose of mentioning these works here is to bring the attention of readers towards forever importance of Otsu's segmentation. [31], organizes his skull stripping procedure as a suit of eight algorithms in which Algorithm 2 is written to obtain an initial mask to obtain rough segmentation of middle brain slice. This procedure comprises of four main steps namely: Otsu's Thresholding, Erosion, Finding Largent connected component and Dilation.

5. RESULT AND DISCUSSION

We have done fully automatic segmentation, classification and volume measurement for ten phantom datasets. Optimization and Segmentation results for subject I, V and X are shown in Table I. Column (1) contains original slices, column (2) contains skull stripped brains, column 3 shows the multimodal histogram of current slice, and column 4 shows how the best threshold is selected using downhill simplex optimization. And finally column (5) provides us with the result and performance of optimization and thresholding. The first three rows correspond to slice 50, 90 and 140 of subject I, which has 1% noise and 20% inhomogeneity. Row number 4, 5 and 6 shown results for subject V, having 5% noise and 20% inhomogeneity. While the last three rows of Table I show results for subject X with maximum noise of 9% and

maximum inhomogeneity of 40%. It is clearly seen skull stripped results in column (1) works fine if a particular slice belongs to the middle of volume and also when the noise and inhomogeneity is low. But if noise and inhomogeneity level is high the skull stripping doesn't work as before which is obviously becomes a problem in automated segmentation of brain. The histograms result in Column (3) also reflect some important observations:

(i)   The extreme and middle slice histograms are not same.
(ii) The clear three peaks in a brain MR histogram belongs to middle of the volume. The peaks and valleys get worse due to noise and INU as shown in subject V and Subject X results in Figure 13.
(iii) Noise and inhomogeneity seriously affects tissue thresholds and densities in a brain volume.
(iv) The histogram is strongly affected by skull stripping step if it is opted as a preprocessing step in brain MR segmentation.
(v)   At extreme slices degenerate input may occur (zero volume) due to bad skull stripping and sparse slices.
(vi) The thresholds decrease as noise in a brain volume increases.

The optimization by Unconstrained Nonlinear Optimization [6] seems quite effective as it finds the minima of error function σ_B^2 which is function of several variables. It would be easily observed in column (4) that at each iteration the threshold vector $[k_1, k_2, k_3]$ points away from the vertex having the highest value of σ_B^2 to the other vertices in the simplex which is tetrahedron in this case. Thus, the direction of search changes via reflection, expansion, inside contraction, outside contraction and shrink operations. We have use following color codes for better visualization of optimization results. The direction of search and step size can be better visualized by projection of 3D simplex onto 2D plane which mostly follow a zigzag pattern. Reader can revise the color code from Figure 14. Hence if the inhomogeneity and noise is below certain level or the brain MR image is improved for bias and partial volume effects. We believe that results would become significantly better than this.

Figure 13 Color Code For Visualization

Finally the column (5) contains thresholds k_1^*, k_2^*, k_3^* along with separability criterion measure $\eta^*(k_1^*, k_2^*, k_3^*)$. The mean of thresholds over ten subject's thresholds measurement where each subject comprises of 181 slices with 217 x 181 voxels per slice is tabulated in Table II. The Discriminant analysis amongst tissues is also supported by variance analysis with p < 0.01 and F >>1 showing there is significant difference amongst the intensities of three tissues. The box plot in Figure 12. confirms this graphically. Note the intensity or gray level L amongst tissues is in the range [0 255].

Table 2 Average Threshold Over Ten Phantom Data Sets

Subject	$\widehat{k_1^*}$	$\widehat{k_2^*}$	$\widehat{k_3^*}$
1	39	108	177
2	37	105	174
3	38	107	173
4	37	105	173
5	39	106	172
6	35	97	164
7	35	100	165
8	34	100	166
9	35	101	166
10	35	101	162

After grouping and labeling via optimization and discriminant analysis we have performed tissue density volume measurements using the process of voxel counting. The volume variability for the three tissue density volumes between 10 subjects are shown in Figure 14(a), (b) and (c) respectively for CSF, GM and WM. Box plot of Figure 14(a) shows that tissue volume densities for CSF in all ten subjects is significantly different. We believe that the outliers for 10 subjects in CSF can be improved via better skull stripping procedure and improving filtering and inhomogeneity effects in MR images. The box plot of Figure 15 (b) shows that difference amongst GM density exists but not as significant as in case of CSF. The density is also much greater than CSF volume density. Finally, the box plot of Figure 15(c) represents WM density volume in the ten subjects showing significant variation in all subjects. In terms of volume density these normal brain phantom data sets contain highest GM density, then WM density and least volume is occupied by CSF voxels.

6. CONCLUSION AND FUTURE WORK

The goodness of thresholds for tissue separation is tested empirically by measure of separability of the tissue gray levels and is found to be varying between 0.90 and 0.99 for every slice of every subject. The discriminant analysis is also supported by ANOVA and significant difference is found with p < 0.01 and F >>1 for the mean gray levels of tissues. Followed by segmentation and classification, volume measurements were also demonstrated for all ten subjects. Amongst 181 slices in each of 10 subjects, the highest volume is occupied by GM voxels and the least volume is occupied by CSF voxels. The sum of tissue volumes over all 10 subjects is also significantly different from each other. Majority outliers appear in CSF voxel count due to partial volume effect and improper skull stripping especially for extreme slices from both ends of each brain volume. Future work incorporates improved skull stripping procedure to separate non- tissue voxels from brain voxel at an initial stage. The experimental results become more robust if noise, inhomogeneity and partial volume effect are addressed in brain MR images before or after skull stripping.
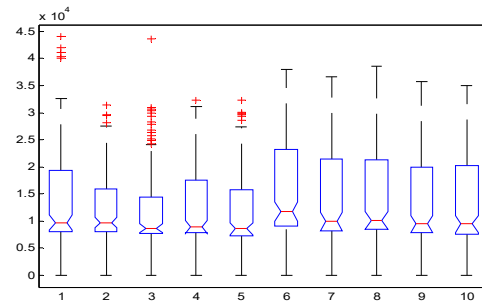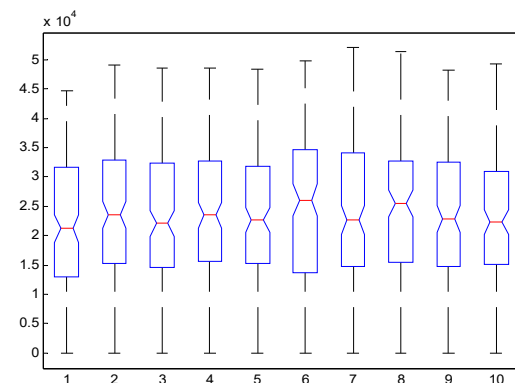

Figure 14 (A) CSF Volume Density In mm^3 For 10 Subjects

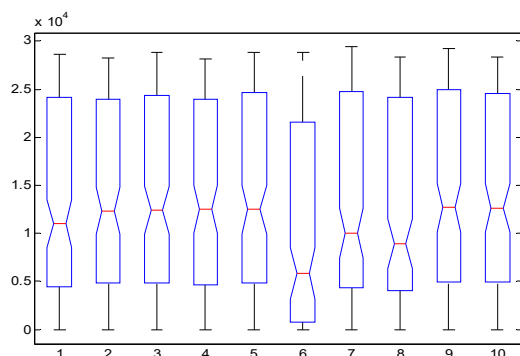*Figure 14 (B) GM Volume Density In mm^3 For 10 Subjects*

Figure *14 (C) WM Volume Density In* mm^3 *For 10 Subjects*

REFERENCES

[1].   N. Otsu, "A threshold selection method from gray level histogram", IEEE Transactins of Systems, Man and Cybernetics Vol.9, 1979, pp. 62-66.

[2].   Henderson, R. G, "Nuclear magnetic resonance imaging: a review". *Journal of th Royal Society of Medicine Volume 76*, 1983, 206-212.

[3].   H.Tariq and A.Burney, "Low Level Segmentation of Brain MR Slices and Quantification Challenges", In 1st National Conference on Mathematics and Computer Science (NCMCS'15), Quaid-e-Awam University of Enginnering and Technology (Pakistan), January 21-23, 2015.

[4].   H.Tariq and A.Burney, "Brain MRI literature review for interdisciplinary studies", Journal of Biomedical Graphics and Computing, Vol. 4, No. 4, 2014, pp. 41-53.

[5].   T. O'Haver, " Peak Finding and Measurement", A Pragmatic Introduction to Signal Processing",University Of Maryland at College Park (USA), terpconnect.umd.edu, 2017.

[6].   J.A Nelder, R. Mead, "A simplex method for function minimization". *The Computer Journal*, 1965, pp.308-313.

[7].   C.Brice, "Scene Analysis using regions", Artifical intelligence, 1970, pp. 205-226.

[8].   D.H.Ballard, C. M. Brown, "Region Growing". In Book Computer Vision, New york, PrenticeHall,1982, pp. 149-165.

[9].   S.W.Zucker,"Survey Region Growing: Childhood and Adolescence", *Computer Graphics and Image Processing*,1976, pp. 382-399.

[10].   N.R. PAL and S. K. PAL, "A Review on Image Segmentation Techniques" Pattern Recogntion,1993, pp. 1277-1294.

[11].   R.C.Gonzales, R.E.Woods. "Digital Image Processing", 2008, Prentice Hall.

[12].   R.M.Haralick and L.G. Shapiro, "Image Segmentation Techniques", *Computer Vision,Graphics and Image Processing 29*, 1985, pp.100-132.

[13].   Dzung L. Pham, C. X, "A Survey of Current Methods in Medical Image Segmentation". *Annual Review of Biomedical Engineering*, 1998, 27.

[14].   M.A. Balafar, A.R.Ramli, M.I.Saripan, S.Mashohor, "Survey of Recent Volumetric Medical Image Segmentation Technique", Springer, 2010.

[15].   M.Sezgin, "Survey over image thresholding techniques and quantitative performance evaluation", Journal of Electronic Imaging, Vol(13), 2004, pp.146-165

[16].   C. Jagath, F.K. Rajapakse, "Segmentation Of MR images with intensity inhomogeneities", Image and vision computing 16, 1998, 165-180.

[17].   V. Leemput, F. Maes, D. Vandermeulen and P.Suetens "Automated Model-Based Bias Field Correction. *IEEE TRANSACTIONS ON MEDICAL IMAGING", VOL. 18*, 1999, 885-896.

[18].   W.M. Wells III, W.E.L.Grimson, R.Kikinis, F.A.Jolesz, "Adaptive Segmentation of MRI Data. IEEE Transactions on Medical Imaging", VOL. 15, No. 4, 1996, pp.429-442.

[19].   J.F. Mangin, "Entropy minimization for automatic correction", Service Hospitalier Frederic Joliot, CEA,2000.

[20].   C. Li, R. Huang, Z.Ding, J.C. Gatenby, D.N.Metaxas, J.C. Gore, "A Level Set Method for Image Segmentation in the Presence of Intensity Inhomogeneities with Application to MRI", IEEE Transactions on Image Processing, VoL.20, No.7, 2011, pp. 2007-2016.

[21].   M. N. Ahmed, S. M, Yamany, N. Mohamed, A.A. Farag and T. Moriarty, "A Modified Fuzzy C-Means Algorithms for Bias field Estimation and Segmentation of MRI Data", IEEE Transactions on Medical Imaging, VOL.21, *No.3*,2002, 193-198.

[22].   D. W. Shattuck, R.Sandoleahy, K.A.Schaper, Rottenberg, R.M. Leahy, "Magnetic

Resonance Image Tissue Classification using a Partial Volume Model", NeuroImage 13, 2001,pp. 856-876.

[23]. A.W.Liew, H. Yan, "Current Methods in the Automatic Tissue Segmentation of 3D Magnetic Resonance Brain Images", Current Medical Imaging Reviews, Vol 2, 2006, pp.1-13.

[24]. L.P. Clarke, R.P.Velthuizen, M.A. Camacho, J.J. Heine, M. Vaidyanathan, "MRI segmentation: Methods and Applications", Magnetic Resonance Imaging, vol 13, 1995, pp. 343-368.

[25]. K.Fukunage, "Introduction to Statistical Pattern Recognition, New York: Academic, 1972, pp. 260-267.

[26]. I. Gresovnik, "Nelder Mead Simplex Method for Unconstrained Minimizatio", Ljubljana, 2009.

[27]. C. A. Cocosco, V.Kollokian, K.Remi, S.Kwan, A.C.Evans, "BrainWeb". Retrieved from Online Interface to a 3D MRI Simulated Brain Database: http://www.bic.mni.mcgill.ca/brainweb/, 1997- May 8.

[28]. A.Buadas, B.Coll, and J.Morel, "A review of image denoising algorithms with a new one", Multiscale modeling and simulation, 2005, pp. 490-530.

[29]. V. M. Jose, C. C. Jose, J.Juan, G. Gracian, and M.L.Montserrat, "MRI denoising using Non-Local Means. Medical Image Analysis", 2008, pp. 514-523.

[30]. B.G. Tabachnick, "Using multivariate statistics (3rd ed.)", New York: Harper Collins, 1996.

[31]. E.Roura, A. Oliver, M.Cabezas, "MARGA: Multispectral Adaptive Adaptive Region Growing Algorithm for brain extraction on Axial J.C. Vilanova, A. Rovira, L.Ramio, X.Llado, "Computer Methods and Programs in Biomedicine, 113(2), 2014, pp 655-673.

[32]. S.Roya, J.A.Butmana, D. L. Phama, "Robust skull stripping using multiple MR image contrasts insensitive to pathology", NeuroImage,2017, pp 132-147.